DYNAMIC THERMOGRAPHY AS AN ADJUNCT TO SURGERY:
Past, Present and Future Applications at Ninewells Hospital, Dundee

Paul Campbell[1], Charlie Song[2], Yeung.Ng[2], Tim Frank[2] & Sir Alfred Cuschieri[2]

[1] *School of Physics and Astronomy, St Andrews University, North Haugh, St Andrews KY16 9SY*
[2] *Department of Surgery and Molecular Oncology, Ninewells Hospital, Dundee University DD1 9SY*

Laparoscopic instrumentation based on energised approaches, such as radiofrequency (RF) current, ultrasonic or laser-based energy sources can considerably expedite many fundamental surgical procedures such as dissection and ligation. Here, heating of the tissue into a distinct temperature regime is required in order to achieve the desired effect, for example, vessel sealing, cauterisation, or cutting. However, this heating requirement is often the source of an added complication: it gives rise to collateral or proximity injury. Electrosurgical damage, for example, is the most common cause of iatrogenic bowel injury during laparoscopic surgery and 60% of mishaps are missed, i.e. the injury is not recognised during surgery and declares itself with peritonitis several days after surgery or even after discharge from hospital. This level of morbidity can have serious consequences, in terms of both the expense incurred by re-admission to hospital, or even the death of the patient. It is our view that all energised dissecting devices may cause thermal collateral damage, especially as the target specific optimum operating parameters are not known. A principal goal of our research thusfar has been to use thermal imaging in order to optimise heating protocols. This article gives a brief overview of our recent, present and future work in this general area of surgical thermography.

1.Overview

Our over-riding concern is that energised surgical instrumentation, whilst advantageous in speeding up various operational procedures, can introduce thermal collateral damage to surrounding healthy tissue, especially when the device power levels are not optimised for the job in hand. We have undertaken *in-vivo* thermal imaging during energised dissection in order to assess, in real time, the optimal power conditions for the successful accomplishment of specific surgical tasks. The main criteria applied are that: (i) the intended procedural step should achieve the correct surgical outcome; (ii) the procedure should introduce the minimum (ideally negligible) of collateral damage to surrounding tissue. In the course of this research it has become clear that, as an adjunct imaging modality, infrared imaging may also improve surgical practice by facilitating easier identification and localisation of tissues such as arteries, especially by less experienced surgeons. As tumours are more highly vascularised than normal tissue, infrared imaging helps facilitate their localisation and staging, that is, the identification of the tumour's stage in its growth cycle. We are also in the process of developing IR endoscopy to address this latter area in a fully laparoscopic context. Pilot research undertaken in an 'open' context (as opposed to the keyhole approach) has served to demonstrate the potential for thermal imaging as an adjunct to energised surgery. This is illustrated well by the in vivo thermographic sequence shown below.

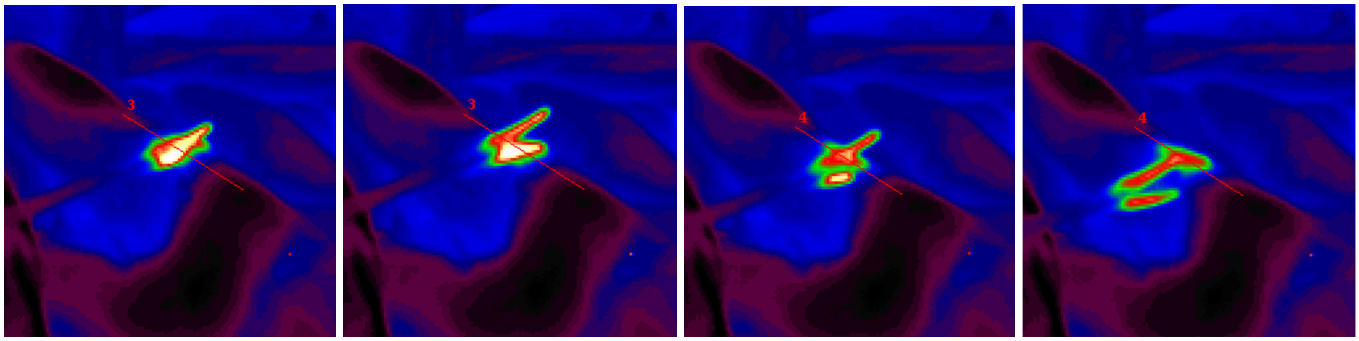

Figure 1: Thermographic sequence taken with the Dundee thermal imaging system and showing: (1) energised forceps attached to bowel, (2) detachment of the forceps revealing hot tissue beneath, (3) removal of forceps, (4) remnant hot-spot extending across the tissue and displaying collateral thermal damage covering 4.5mm either side of the instrument jaws. [see also AVI-1 in the Appendix]

2. Previous Thermal Imaging Work

2.1 Shape Memory Alloy Staples

In a medical context, thermographic techniques are most often associated with the assessment of peripheral vascular disease [1]. However, the Dundee Surgical Technology Group's initial interest has been in the application of thermography to the optimised deployment of heat activated surgical staples

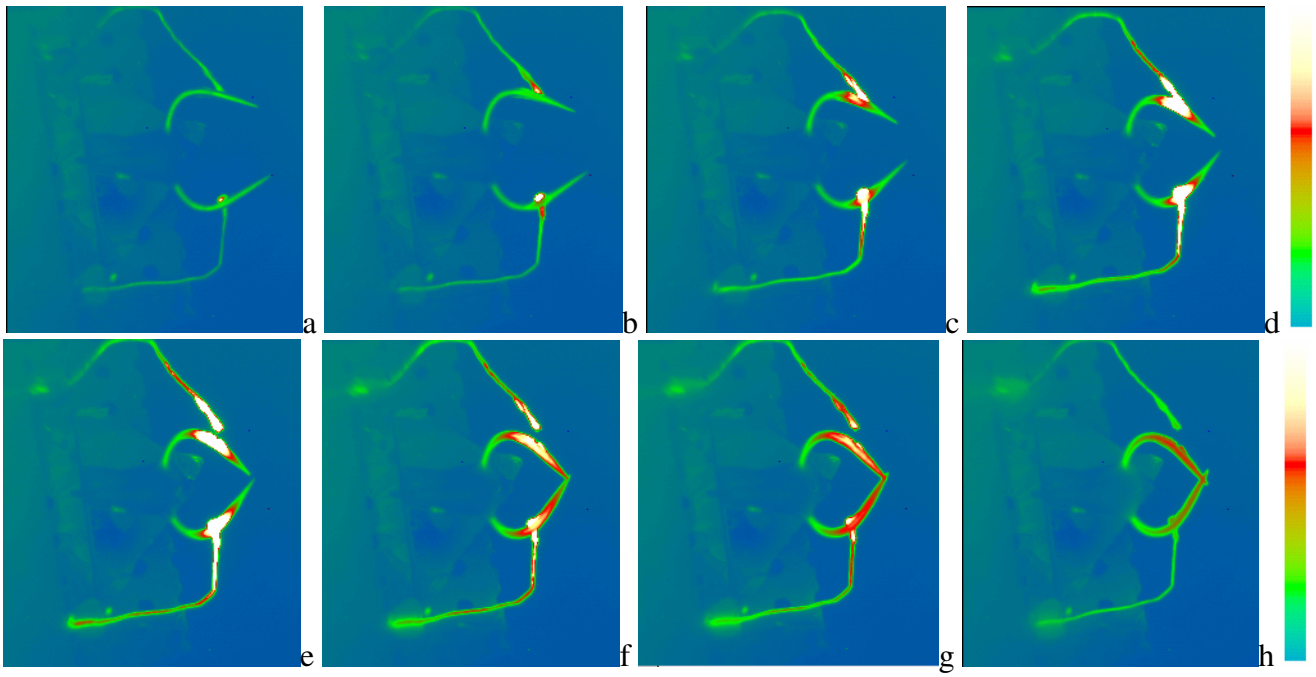

Figure 2. Thermal activation of shape memory alloy suture staples captured using our high specification infrared imaging camera. Resistive heating by a current pulse [2amp/160millisecond] causes the 'C' shaped staple to close. The timings from pulse initiation are: t = 0, 0.02, 0.1, 0.16, 0.24, 0.3, 0.35 & 0.6 seconds and the temperature scale runs from 23.4ºC (dark blue) to 79.1ºC (white). [As an aid to gauging the scale of the view, the backbone of the staple is 5mm in length.]

that we had developed in-house. All our thermography work is undertaken with a state-of-the-art Raytheon thermal imaging camera system (Radiance HS). Figure 2 shows eight frames from a typical time-lapse thermography sequence acquired using the thermal camera in combination with a close-up lens capable of 100 µm pixel resolution. Timings are taken relative to the initiation of the current pulse, with the first frame in the sequence of figure 2 captured just as the current begins. Small hot spots are seen to develop at the contact points between the current supply wires and the staple [2]. These are generated due to the marked difference in resistance at the interface and actually serve our purposes well as this enhanced localised heating is targeted at the regions of the SMA staple in which most internal strain is stored. This particular sequence also highlights another crucial factor in dictating the overall dynamics of heat flow through the staple system: it can be seen in frame (e) above that the contact rail that supplies current to the upper half of the staple becomes detached during the sequence and subsequently heat is retained in the the upper region of the staple compared with the lower section, in which good thermal contact is maintained. The take home message from this observation is that the heat sink effect of contact /holding rails in a fully developed prototype is critical to extracting heat energy away from the tissue interface. We later used thermal imaging in a similar context to optimise the deployment of staples from the actual prototype (*viz section 3 below*).

2.2 Finite Element Analysis

During temperature activated staple closure, heat may be conducted into the surrounding tissue. In order to minimise any resultant collateral tissue damage, a computational thermal analysis is required to establish the desirable duration of heating and the subsequent temperature distribution within the surrounding tissue. We have been active in the development of clinically relevant finite element based

analyses of our heat activated SMA staples [3]. This section gives an overview of the pertinent mathematics and our assumptions on the boundary conditions that we apply to the models.

In practice, the backbone of the SMA staple design is resistively heated by electric current, as shown in figure 2 above. Heat will conduct into the legs of the staple, subsequently flowing from the legs into the surrounding tissue. The backbone will be in contact with a combination of tissue, body fluid, supply rails, and air, although the relative extent of these contacts will generally be indeterminate and must be fitted empirically [4]. In the thermal analysis, we assume that these properties approximate to those of water. It is notable that the thermal conductivity and diffusivity of NiTi alloy (from which the SMA staples are constructed) are about two orders of magnitude greater than those for water. We therefore considered it important to compare the linear conduction of heat from backbone into legs with radial conduction from the backbone and legs into the surrounding tissue.

The differential equation of linear heat flow along the *x* co-ordinate is

$$\frac{\partial T}{\partial t} = \kappa \frac{\partial^2 T}{\partial x^2} \tag{1}$$

The finite difference representation of this equation is

$$T_{i,j+1} = T_{i,j} + \kappa \frac{\delta t}{\delta x^2}\left[T_{i-1,j} - 2T_{i,j} + T_{i+1,j}\right] \tag{2}$$

where T is the absolute temperature, $\kappa = k/\rho c$ is the thermal diffusivity, δt is the computation time increment, δx the distance increment, i the time step counter, and j is the distance step counter.
Using the same notation, the equation for radial heat flow along the *r* co-ordinate is

$$\frac{\partial T}{\partial t} = \kappa\left(\frac{\partial^2 T}{\partial r^2} + \frac{1}{r}\frac{\partial T}{\partial r}\right) \tag{3}$$

The finite difference representation of this equation is

$$T_{i,j+1} = T_{i,j} + \kappa \frac{\delta t}{2i\delta x^2}\left[(2i+1)T_{i+1,j} - 4iT_{i,j} + (2i-1)T_{i-1,j}\right] \tag{4}$$

These equations were solved using the finite difference method to give temperature distributions against time for linear and radial conduction respectively. The programs were written in Matlab

Note that since the modes of heat transfer are different along the length of the SMA staple and from the staple legs to surrounding tissues, it is necessary to perform a 3D thermal analysis to understand the thermal diffusion along the complex geometry of this system.

The most general partial-differential equation for 3D heat conduction is of the form

$$\frac{1}{\kappa}\frac{\partial T(\hat{r},t)}{\partial t} = \nabla^2 T(\hat{r},t) + \frac{g(\hat{r},t)}{k} \tag{5}$$

where g(r,t) is a function describing the rate of heat generation rate per unit volume in the system, **r** is the spatial vector.

Equation (5) was used in the finite element discretisation to build up the 3D staple-tissue model. For simplicity, we assume that all the thermal properties of SMA wire are linearly dependent on temperature. The programs were written using ANSYS, which is a dedicated finite element analysis package. A 20-node brick element was selected to model the irregular geometry and curved boundaries. Since the staple has two planes of symmetry dividing it into quarters, we undertake the calculation on one such portion only to ease the computational burden.

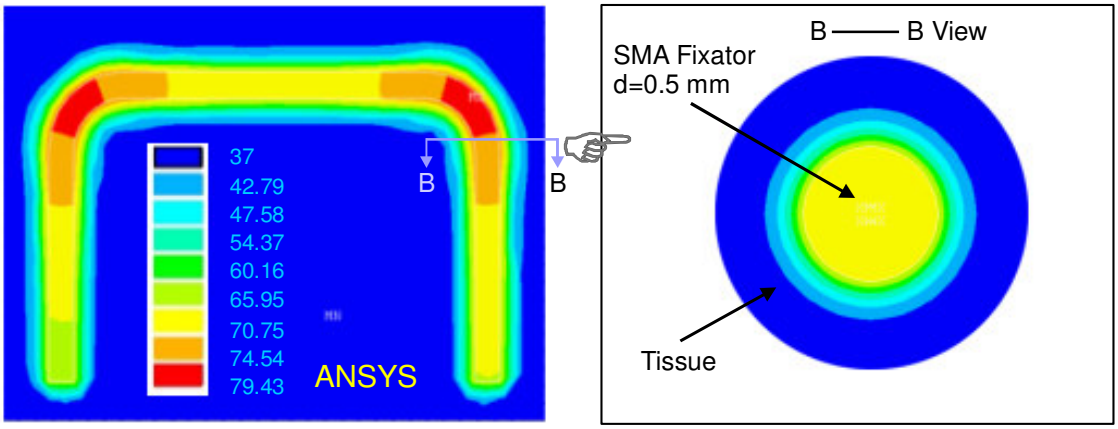

a) b)

Figure 3. Temperature distribution within the fixator and tissue [See also AVI-2 and AVI-3 in Appendix 1]

We have used this preliminary model in order to ascertain the dynamic temperature distribution after current heating, as shown in Figure 3a, and the axial view temperature pattern of one leg is shown in Figure 3b. The simulations of the heat flow have been built for both view directions. The heating effect within the tissue is confined to a layer 0.05 mm thick (Figure 3a), considering the geometric effect at the corners, the most affected area is limited to within 0.5 mm of the staple (Figure 3b). By the end of the first time interval of (0.005 s), the tissue-staple interface temperature has dropped significantly [3]. This shows that cooling at the interface is so rapid that the tissue is not heated significantly, so long as the pulse duration is of the order of 0.1s.

3 Current Research Programme

Our main efforts are concentrated on two fronts at present:
(i) In-vivo Studies using a range of standard energised surgical equipment (ultrasonic and electro-based);
(ii) Optimisation of SMA Stapling Device.

3.1 In vivo research

The group have already conducted two in-vivo thermography studies in order to ascertain the level of thermal spread (and associated collateral damage) during open energised surgery [5]. For example, the thermographic sequence of figure 1 on page 1 illustrates how thermal spread may be monitored during instrument activation period. Figure 4 shows a different sequence whereby a bipolar vessel sealing system (Ligasure LS1100-Atlas: Tyco Healthcare) is imaged during activation on the short gastric tissues. A normal view of the instrument is shown in figure 4(f): there is no indication of the device surface temperature, nor is there any clue to the thermal spread generated by the instrument. The thermal imaging sequence of the power activation process is shown in figures 4(a-e). Initially there is little contrast between the instrument head and the exposed tissue as they are at similar temperatures 4(a), however when the pulse is activated 4(b), a thin region of higher temperature emanates from the periphery of the device head. The lateral width of the heated region is low in comparison with other devices reported in the literature, and it remains confined throughout the duration of activation. If a linear region of interest (LROI) is generated, as indicated by the white line highlighted on figure 4(a), then the temperature history of that profile can be examined quantitatively (as illustrated in figure 4(g)) and a measure of the maximum thermal spread obtained from the 2D projection (as shown in figure 4(h). From the 3D graph in

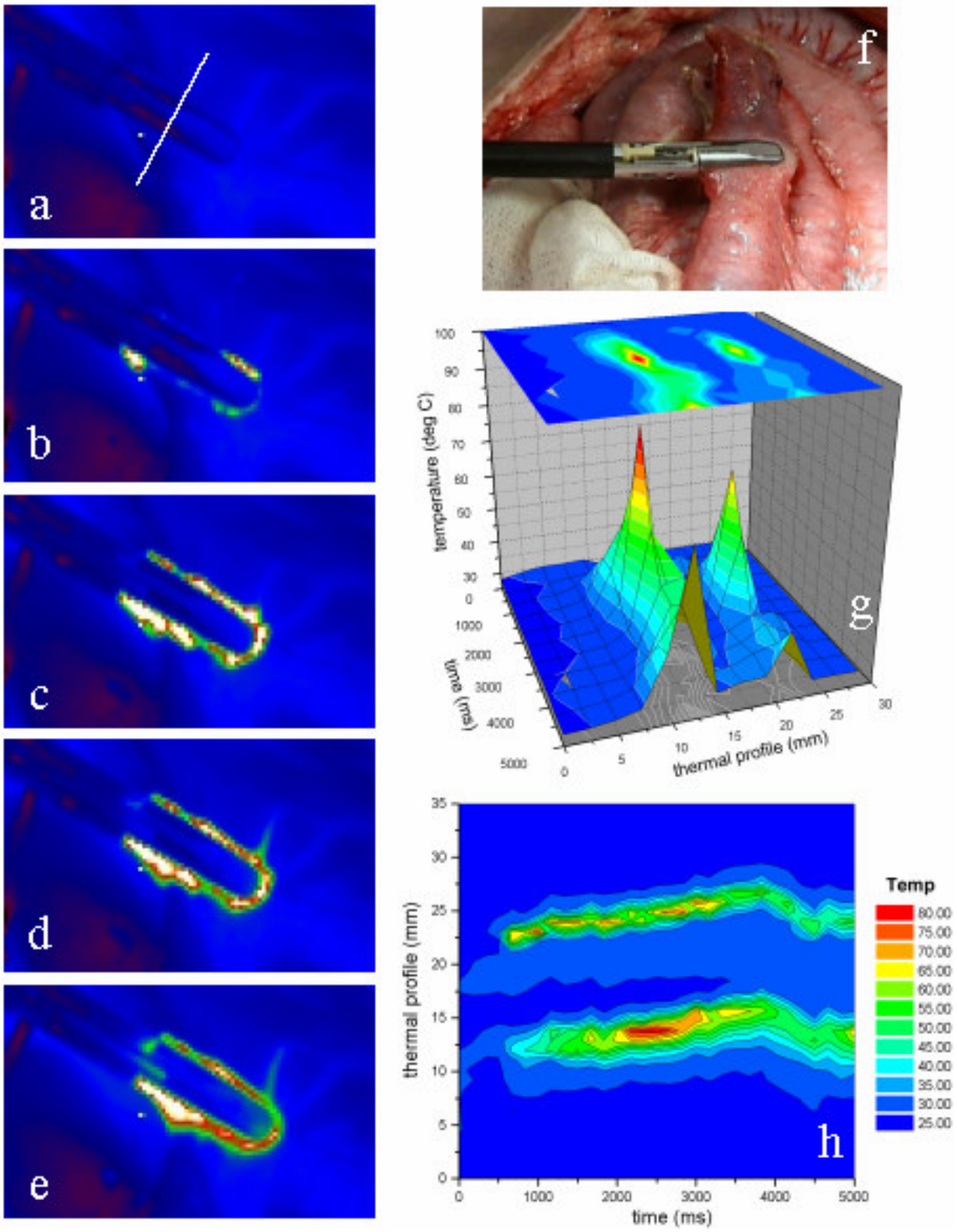

Figure 4 (a-e). [see also AVI 4 in the Appendix]. Thermal imaging sequence showing activation of the LS1100 (10mm Laparoscopic 'Atlas') device on the short gastric tissue. The respective timings for each frame, as indicated from the horizontal axis on figure 4(h), are: 0 ms; 462 ms; 633 ms; 1416 ms; and 3898 ms. The LS1100 does not become as hot as comparable commercial devices operating with similar power levels during activation. This makes the device significantly less likely to introduce iatrogenic injury. (f) Image of the of the device taken at wavelengths visible to the naked eye. (g) 3D thermal profile mapped according to the linear region of interest highlighted by the white line in figure 4(a). (h) Contour plot of the thermal data showing that the maximum thermal spread either side of the device is about 3mm on this occasion.

figure 4(g), it is clear that the temperature rises to just over 80ºC after 1.2s, and then stabilises at a lower temperature until the end of the pulse. Importantly, the temperature rise on the actual device head does not exceed 35ºC throughout the activation period, in stark contrast to the performance of comparable instruments that, whilst operating with similar power settings, can result in surface temperatures of well over 100ºC. Tandem histological studies confirm that detectable collateral damage is slightly less than that estimated using thermography. This is because physical damage to tissue is not only a function of the maximum temperature to which tissue is exposed, but rather the time integrated temperature over the duration of the power pulse. The added benefit to the surgeon from a real-time video feed provided by *in situ* thermography is that the thermal images allows immediate appreciation of instrument temperature and this visual cue automatically alerts to the potential for iatrogenic injury (if for example, a hot instrument should come into close contact with any vital structures). By the same token, the *in situ* thermal image also indicates when the surface of the instrument has cooled to ambient temperature and may thus be 'parked' safely, especially when undertaking keyhole surgery.

Dynamic infrared thermography also allows instant examination of the integrity of haemostasis produced by an energised device. This is because the rate of local cooling in the sealed tissue (after removal of the device head from the field of view) is distinctly different from that of the tissue immediately surrounding the affected region. This is demonstrated below, where a thermal profile through a tissue hot-spot has been monitored as a function of time, and in which it is clear that the central region of the hot-spot (from 7.1-8.5mm on the y-axis (figure 5a)) cools more rapidly than the immediate locale. This indicates that a transformation of tissue thermal properties has indeed occurred, as is desireable. This information thus affords the surgeon the knowledge that the requisite tissue structural change is complete, the seal is good, and it is safe to proceed. Notably, the data acquisition time required to perform such analysis is very fast, taking only around 1 second. We are pursuing this aspect of the research in order to arrive at quantitative values for the cooling constants on different target tissues. The facility to implement this level of security during a keyhole operation would significantly reduce the risk involved each surgical procedure. A finite element model of the sealed vessel cooling effect has also been developed to compare with the experimental result and to illustrate that the differntial cooling is dominated by a transform in tissue properties rather than the altered tissue morphology (fig 5b).

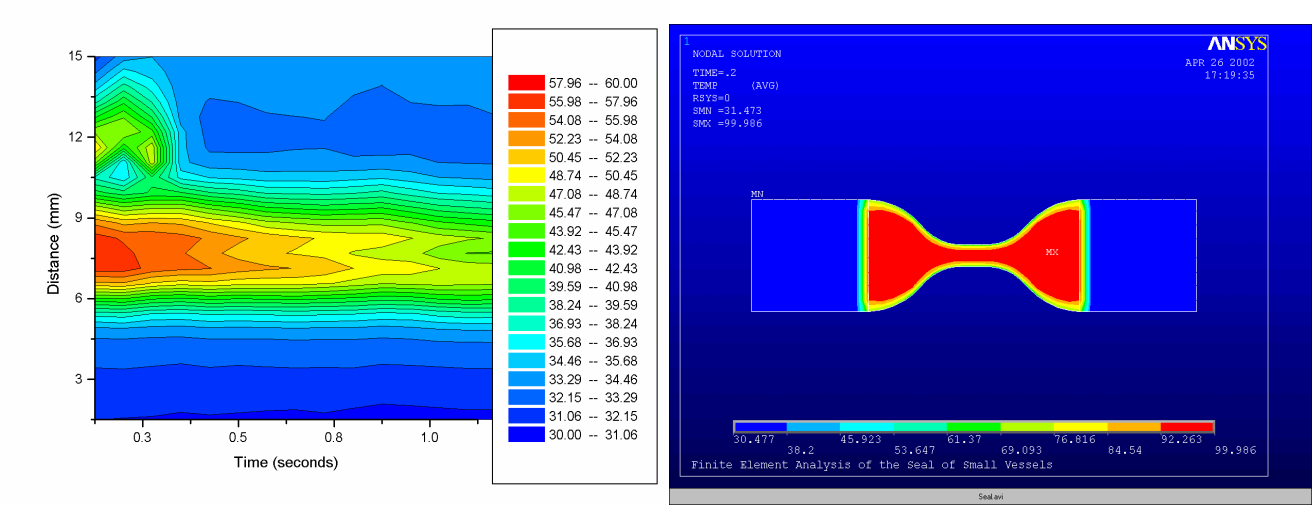

Figure 5 (a) Temporal evolution of a thermal profile taken through a tissue hot-spot (a seal on a vessel) after removing the electro-surgical instrument from the field of view (this data has been extracted from the cooling hotspot in figure 1d). (b) Finite element construction of the cooling seal viewed side on (viz AVI 5 for a dynamic view of the modelled cooling process). We intend to automate the image processing required to generate plots such as that in 5(a) so that an immediate check on seal quality is available to the surgeon allowing him to quickly proceed with the operation without fear of causing accidental bleeds.

3.2 Optimised Staple Deployment

A combined applicator/ heater device has been designed to deploy the SMA staples mentioned earlier. This again utilises electrical resistance heating along the staple backbone through application of electrical current via electrodes with a custom groove in which the staple corners sit. The timing of the electrical current is governed using a monostable circuit providing an adjustable electrical pulse of between 25-250ms. An integral rechargeable 2V source provides a current of 5.71A.

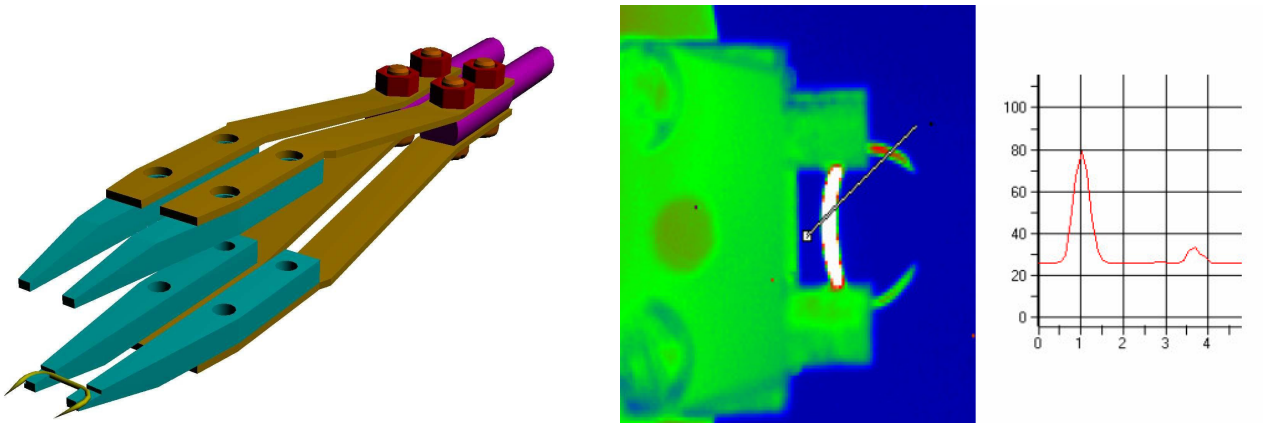

(a) (b)

Figure 6. (a) Schematic of the staple deployment device and (b) In-situ thermogram showing the hot backbone clamped between the brass contacts. The inset to (b) is a thermal cross-section as indicated by the white line in (b) and illustrates that the backbone temperature is raised sufficiently that the shape memory recovery is effected, but heat transfer down the legs (and thus into tissue) results in a temperature rise of a mere 7ºC above ambient levels.

4.1 Infrared Endoscopy

The level of UK/European activity in the specific area of infrared endoscopy is negligible. Indeed, there have only been a handful of relevant reports in the entire literature. Originally, attempts were made to achieve coupling from the target internal tissues to a detector on the outside via infrared transmitting optical fibres [6], but the resolution that is achievable by this method remains poor, and certainly well short of that required for surgical guidance or for diagnosis.

A report originating from a surgical group at Johns Hopkins University [7] has indicated that physiological parameters such as perfusion, which is not accessible with visible light endoscopy, can be successfully assessed when operating in the infrared. The identification of anatomical structures was also more easily achieved, even for novice endoscopists, compared with conventional visible endoscopy. Although the architecture of the instrument was not specified, their findings underscore the potential applicability of infrared endoscopy. We intend to achieve a similar observational capability by utilising our existing state-of-the-art thermal imaging hardware as the detection mechanism and channelling infrared radiation to this via an IR transmitting optical relay stage (after the fashion of the relay stage

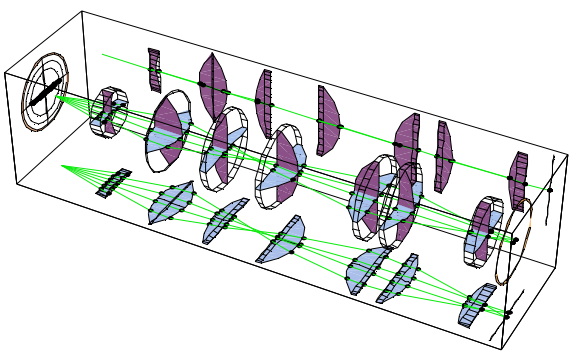

Figure 7. Optica (for Mathematica) model of a single stage white light relay.

shown in figure 7 below.). The instrument will be designed along the lines of the Hopkins rod-lens architecture [8] with suitable modification to account for the altered refractive index of Si/Ge optics compared with standard white light lenses. The initial prototype will be operational by 2004. The main thrust of this project will be to elucidate the following key goals:

(i) to explore the possibility of observing thermal spread from energised electrosurgical instrumentation and to minimise this through direct observation via the infrared channel;
(ii) to attempt fast localisation of particular anatomic structures via thermal imaging of their vascular infrared signature;
(iii) to assess directly any effect of tissue perfusion, particularly of the small and large intestine:
(iv) direct detection and staging of intra-abdominal tumours or focal intra-abdominal sepsis/ inflammation also becomes possible as such regions exhibit different (higher) temperatures from surrounding healthy tissues;
(v) targeted fluorescence spectroscopy with non-cytotoxic infrared excitation in a shared aperture mode.

The fully developed prototype will also allow the thermographic image to be overlaid on the conventional white-light image, so that the surgeon's view is both enhanced and optimised.

Conclusions

The Surgical Technology Group at Ninewells have developed expertise with thermal imaging as an adjunct to surgery. This encompasses the use of in-house developed heat activated staples for use in keyhole surgical suturing; in-situ thermography during energised surgery; and presently, the development of infrared endoscopy. Further details of all our projects are available at the departmental web-site: www.dundee.ac.uk/surgery.

This work was supported by the Wellcome Trust (Grant 009572). 1999, and also the EPSRC (Grants: GR-S09951/01 (2002) and also GR-S00026-01 (2002).

For copies of reprints, or with other queries relating to this work, please contact
Paul Campbell on 01382 496361 [p.a.campbell@dundee.ac.uk]

References

[1] B.F.Jones, ***IEEE Trans. Med. Imag***. 17 (6) 1019 (1998)
[2] P.A.Campbell, C.Song, T.G.Frank & A.Cuschieri ***Thermology International*** 11 (2), 5 (2001)
[3] C Song, P A Campbell, T G Frank, and A Cuschieri ***Smart Materials and Structures*** 11(3), 1 (2002*)*
[4] Y. Ng, C.Song, D McLean, S. Shimi, T.G.Frank, A.Cuschieri & P.A.Campbell. Submitted to ***Applied Physics Letters*** (2003)
[5] P A Campbell, AB Cresswell, T G Frank and A Cuschieri. ***Surgical Endoscopy*** *(accepted for publication in 2003)*
[6] K. Mabuchi et al: p98 ***The Thermal Image in Medicine and Biology***. Uhlen (Vienna 1995) [Eds EFJ Ring and K. Ammer]
[7] W. Roberts, L. Kavoussi, et al. ***Surgical Endoscopy*** 11, 1221-1223 (1997)
[8] H Hopkins, in ***Endoscopy*** (Chapters 1 & 2) (Edited by G. Berci)

Appendix

Click on the images below to view real time AVIs relating to the figures above.

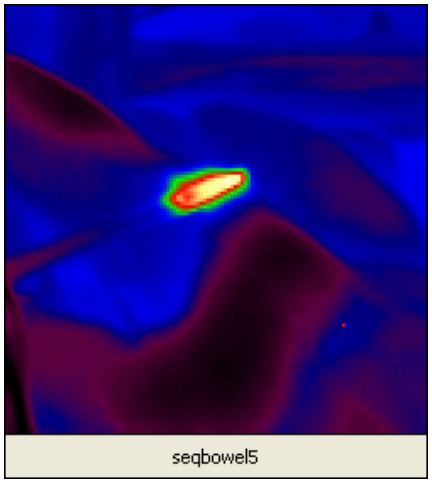

AVI-1: thermographic sequence showing detachment of hot forceps.

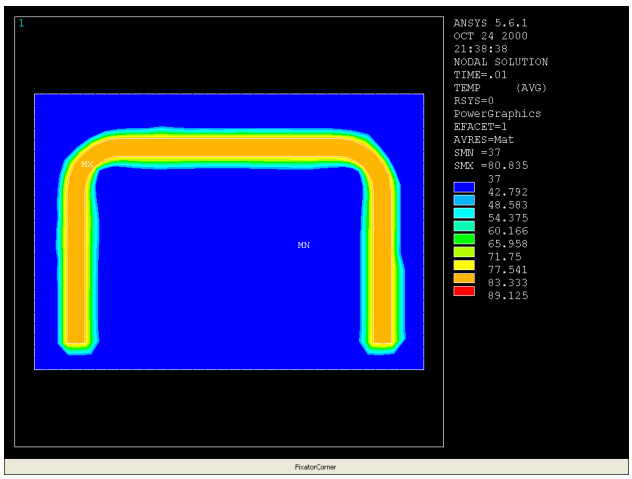

AVI-2 FE modelled heating and cooling of the SMA staples.

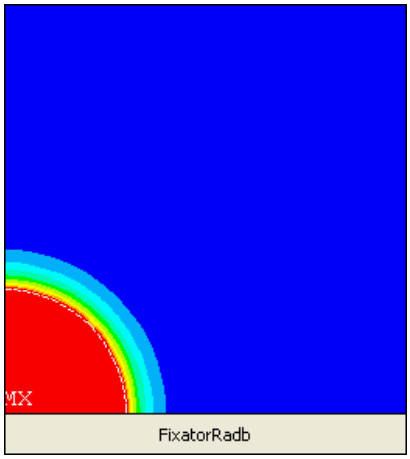

AVI-3 Radial evolution of heat deposited from the current activated staple.

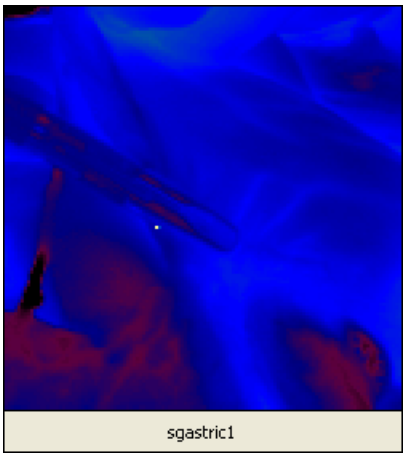

AVI-4 Thermography sequence of activated Ligasure LS1200 on short gastric target tissue.

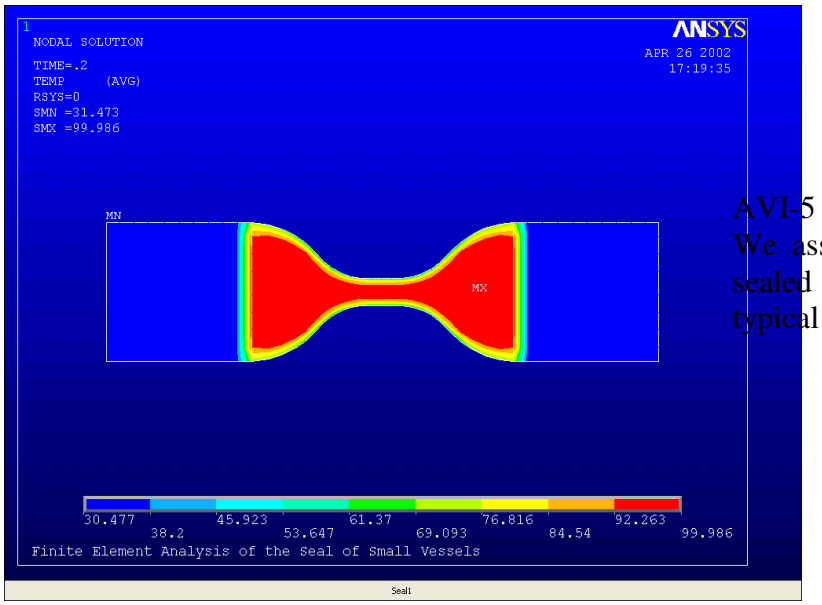

AVI-5 FE modelled cooling of a sealed region. We assume that the material properties of the sealed tissue closely approximate that of a typical plastic.